Title
Flexible tethering of primase and DNA Pol α in the eukaryotic primosome.

Journal
Nucleic acids research, 39(18)

ISSN
0305-1048

Authors
Núñez-Ramírez, Rafael
Klinge, Sebastian
Sauguet, Ludovic
et al.

Publication Date
2011-10-01

DOI
10.1093/nar/gkr534

Peer reviewed

Published online 28 June 2011 *Nucleic Acids Research, 2011, Vol. 39, No. 18* ***8187–8199***
doi:10.1093/nar/gkr534

Flexible tethering of primase and DNA Pol α in the eukaryotic primosome

Rafael Núñez-Ramírez[1], Sebastian Klinge[2], Ludovic Sauguet[2], Roberto Melero[1], María A. Recuero-Checa[1], Mairi Kilkenny[2], Rajika L. Perera[2], Begoña García-Alvarez[1], Richard J. Hall[3], Eva Nogales[3], Luca Pellegrini[2,*] and Oscar Llorca[1,*]

[1]Centro de Investigaciones Biológicas, Consejo Superior de Investigaciones Científicas (CSIC), Ramiro de Maetzu 9, 28040 Madrid, Spain, [2]Department of Biochemistry, University of Cambridge, Tennis Court Road, Cambridge CB2 1GA, UK and [3]University of California, 742 Stanley Hall, MS 3220, Berkeley, CA 94720-3220, USA

Received April 14, 2011; Revised May 20, 2011; Accepted June 12, 2011

ABSTRACT

The Pol α/primase complex or primosome is the primase/polymerase complex that initiates nucleic acid synthesis during eukaryotic replication. Within the primosome, the primase synthesizes short RNA primers that undergo limited extension by Pol α. The resulting RNA–DNA primers are utilized by Pol δ and Pol ε for processive elongation on the lagging and leading strands, respectively. Despite its importance, the mechanism of RNA–DNA primer synthesis remains poorly understood. Here, we describe a structural model of the yeast primosome based on electron microscopy and functional studies. The 3D architecture of the primosome reveals an asymmetric, dumbbell-shaped particle. The catalytic centers of primase and Pol α reside in separate lobes of high relative mobility. The flexible tethering of the primosome lobes increases the efficiency of primer transfer between primase and Pol α. The physical organization of the primosome suggests that a concerted mechanism of primer hand-off between primase and Pol α would involve coordinated movements of the primosome lobes. The first three-dimensional map of the eukaryotic primosome at 25 Å resolution provides an essential structural template for understanding initiation of eukaryotic replication.

INTRODUCTION

Initiation of nucleic acid synthesis during replication presents a unique challenge to the cell, as DNA polymerases can only extend the 3′-end of an existing DNA chain, but cannot initiate synthesis *de novo*. A specialized DNA-dependent RNA polymerase, termed primase, is responsible for synthesizing the short RNA primers that are utilised by the replicative DNA polymerases (1,2). The antiparallel arrangement of the strands in the DNA double helix means that initiation events must take place repeatedly on the lagging strand, to prime synthesis of each Okazaki fragment. Indeed, the enzymatic activity of the primase is constantly required at the replication fork (3).

Primases synthesise oligoribonucleotides that are 7–12 nt in length. In the absence of DNA polymerase, primases can extend the primer by multiple rounds of unit-length elongation. Prior to ligation of a newly synthesized Okazaki fragment to the nascent DNA chain, the RNA primer is normally removed (4). In bacteria, the primase is a single polypeptide whereas in archaea and eukaryotes the primase is a heterodimeric enzyme comprised of a small subunit PriS endowed with catalytic activity and a large subunit PriL with multiple regulatory functions (5,6). The conserved C-terminal sequence of PriL (PriL-CTD) is an iron–sulfur cluster domain with an important functional role in RNA primer synthesis (7,8). In eukaryotes the primase is found tightly associated with Pol α and its B subunit in a heterotetrameric complex, the Pol α/primase complex or primosome (9).

*To whom correspondence should be addressed. Tel: +34 918373112 (Ext. 4446); Fax: +34 915360432; Email: ollorca@cib.csic.es
Correspondence may also be addressed to Luca Pellegrini. Tel: +0044 1223 760469; Fax: +0044 1223 766002; Email: lp212@cam.ac.uk
Present addresseses:
Rafael Núñez-Ramírez, Instituto de Estructura de la Materia, CSIC, Serrano 113bis, 28006 Madrid, Spain.
Sebastian Klinge, Institut für Molekularbiologie und Biophysik, ETH Zurich, CH-8093, Switzerland.
Ludovic Sauguet, Département de Biologie Structurale et Chimie, Institut Pasteur, 75724 Paris CEDEX 15, France.
Begoña García-Alvarez, Universidad Complutense de Madrid, Madrid, Spain.

The authors wish it to be known that, in their opinion, the first two authors should be regarded as joint First Authors.

Once the RNA primer has reached its full size, the primase must hand it over to the DNA polymerase for processive elongation. In eukaryotic replication, the hand-off between primase and polymerase takes place within the primosome: the 3′-end of the RNA primer is transferred intramolecularly to the active site of Pol α for limited extension with dNTP. The resulting RNA–DNA primer is then handed over to Pol δ and Pol ε on the lagging and leading strand, respectively, in a process that requires the clamp loader Replication Factor C and the sliding clamp PCNA (10).

A detailed structural characterization of the primosome is still lacking and consequently our understanding of the mechanism of initiation of nucleic acid synthesis is very limited. Pol α shares with Pol δ and Pol ε a conserved core comprising a catalytic subunit and the B subunit (11). In addition, each polymerase has a collection of unique accessory subunits. The sequence conservation of the catalytic subunit extends beyond the polymerase domain to a cysteine-rich C-terminal domain (αCTD) that mediates the interaction with the B subunit. An initial framework for the structural core of the three replicative polymerases has been provided by combining the 3D-electron microscopy (3D-EM) structure of the Pol α–B subunit complex with the X-ray crystal structure of the carboxy-terminal domain of Pol α (αCTD)–B subunit complex (12).

Available crystallographic models of the catalytic PriS subunit of the archaeal primase, which is related to the eukaryotic primase, show that its polymerase fold has found widespread adoption in such functionally diverse molecules as the eukaryotic Pol X family of DNA polymerases and the multi-functional bacterial DNA end-joining polymerases (6,13). The only available primase structure that includes both PriS and PriL subunits shows that the heterodimeric primase is a very elongated molecule (5). Currently, no structural information is available for the eukaryotic primase with the exception of the conserved carboxy-terminal domain of its large subunit (PriL-CTD), a Fe-S cluster domain with a critical role in the initiation of an RNA primer synthesis (7,8,14,15).

Here, we describe the first three-dimensional (3D) model of the primosome from *Saccharomyces cerevisiae*, obtained by electron microscopy (EM) analysis of the recombinant complex. The outstanding feature of the structure is the large physical separation between the catalytic centers of primase and Pol α, which reside in separate lobes of a highly flexible dumbbell-shaped primosome particle. This flexibility results from the interaction of the primase with the Pol α–B subunit complex (12). We provide functional evidence that such architectural organization contributes to increase the efficiency of the internal primer hand-off between primase and Pol α. The complete structural template for the yeast primosome provides the first insight into how primase and Pol α cooperate in the production of the RNA–DNA primer required for genome duplication in eukaryotic replication.

MATERIALS AND METHODS

Preparative biochemistry

Primosome. Amino acids 349–1468 (C-end) of Pol α, fused to a N-terminal StrepII tag, and amino acids 246–705 (C-end) of the B subunit were co-expressed in Sf9 insect cells as described (12). The primosome was reconstituted by mixing the lysate of insect cells overexpressing the Pol α–B subunit complex with purified primase. The reconstituted primosome was purified by affinity chromatography over a Strep-Tactin sepharose column and by heparin sepharose chromatography. All purified protein samples were flash-frozen in liquid nitrogen and stored at −80° in small aliquots. All samples were gel-filtered in preparation for electron microscopy analysis.

Prim complex. The Prim complex was reconstituted over gel filtration by combining purified samples of primase and αCTD–B subunit complex. The αCTD–B subunit complex was overexpressed and purified as described (12). The truncated version of the Prim complex lacking the PriL-CTD, Prim$L_{\Delta CTD}$, was reconstituted in the same way, using truncated primase.

Primase. The yeast primase was produced in Rosetta 2 (DE3) *Escherichia coli* strain using the vector pRSFDuet-1 vector expressing full-length PriS and His-tagged PriL (49–513). The first 48 amino acids of PriL were omitted as they are not conserved and are likely to be disordered. The primase was purified by Co-NTA agarose chromatography, heparin sepharose chromatography, His-tag cleavage and removal and gel filtration chromatography. A truncated version of the primase, lacking amino acids 336–513 of PriL, was prepared according to the same purification protocol.

Polα_{cat}. The polymerase domain of Pol α, spanning amino acids 349–1258, was expressed as an N-terminal, dual His-strepII tag from pRSFDuet-1 vector in Rosetta 2 (DE3) *E. coli* strain and purified by Co-NTA agarose, heparin sepharose, Strep-Tactin sepharose and gel filtration chromatography.

Electron microscopy and 3D reconstructions

The primosome, Prim complex, PrimΔL_{CTD} complex and primase samples were analyzed by electron microscopy after being adsorbed to glow-discharged carbon coated grids and stained with 2% uranyl formate. Grids were observed using a JEOL JEM-1230 transmission electron microscope operated at 100 kV and a nominal magnification of 50 000. Micrographs were obtained under low dose conditions and digitized at a final pixel size of 4.2 Å. Primase samples were recorded using a TVIPS CMOS 4kx4k camera at the same magnification. The contrast transfer function of the microscope for each micrograph was estimated using CTFFIND3 (16) and corrected using Bsoft (17). A total of 17 628, 11 088, 7210 and 4450 images of the primosome, Prim complex, PrimΔL_{CTD} complex and primase, respectively, were manually extracted using EMAN (18) (see Supplementary Figure S1 and Supplementary Table S1, for details on the image

processing). Only side-views, corresponding to different projections along the longitudinal axis of the complexes, were selected. These side views are sufficient to cover Fourier space and the use of side-views only to obtain a correct reconstruction is the standard in many cases, such as the GroEL chaperonin (19). 2D reference-free classification and averaging for each of the data sets was performed using EMAN (18), XMIPP (20) and maximum-likelihood methods (21). Angular refinement was performed using EMAN and several starting templates, including several synthetic Gaussian blobs based on the reference-free 2D averages and the Pol α–B subunit complex map filtered at low resolution (12) (Supplementary Figure S2). Refinement converged to similar reconstructions using different starting references. The data of the full primosome did not converge initially due to conformational heterogeneity, which was solved by splitting the data set into more homogenous subgroups following a strategy described below. In all cases and after convergence, we compared projections of the structures solved with the reference-free averages and their good agreement supported the correctness of the final structures. The heterogeneity in the conformations of the Prim complex was analyzed using 3D maximum-likelihood (ML3D) classification (22). The handedness of the reconstruction of the primosome was defined after fitting of the atomic structure of the related archaeal polymerase (unpublished PDB entry: 3A2F) into the Pol lobe of the primosome. Only one hand provided an adequate fitting and this was selected for the rest of the structures.

The structure of the αCTD–B subunit complex (PDB entry: 3FLO) was fitted into the reconstruction of the Prim complex using unbiased computational methods as provided by ADP_EM (23). The output solutions obtained using ADP_EM were then locally refined using UCSF Chimera (24). These fitting experiments also permitted defining the correct handedness of the reconstruction as the one providing a higher correlation with the fitted structure of the αCTD–B subunit complex (PDB entry: 3FLO). The fitting solutions with the higher scores for one of the two possible hands of the reconstruction (the one shown in results) showed much higher cross-correlations that any of the best solutions for the opposite hand (cross-correlation > 0.6 for one hand, compared to 0.3 for the opposite hand). The resolution of the structures, calculated using a 0.5 cut-off of the FSC, was 25 Å and ~22 Å for primosome and Prim complex, respectively. The final volumes and fitting were visualized using UCSF Chimera (24).

Analysis of conformational flexibility of the primosome

A multi-reference 3D angular refinement was performed to obtain a structure of the primosome despite its conformational heterogeneity, using the 'multirefine' command in EMAN (18) and a strategy defined before (25). Each primosome image in the data set was compared to all projections from three 3D references, and each image was assigned to that structure and orientation with the best correlation. One reconstruction out of the three obtained in each round of refinement showed the best connectivity between lobes and this was then used as 3D reference for the following step. In each round, three slightly different starting models to seed the refinement were built by adding random noise to the selected reconstruction, following methods described before (25). We observed that refinement progressed adequately only if the particles assigned to the structure with the best connectivity were split and only these used for subsequent rounds. This subset of particles was again reclassified and split into three subgroups and only the subset showing good connectivity was allowed to progress to the next round of refinement. This process was repeated iteratively until it converged upon a subset of 3129 particles that stably produced one reconstruction with a defined connecting linker. These images were then processed independently to remove any bias of the classification procedure. Attempts of classification using ML3D (22) were unsuccessful, likely due to the coexistence of a large number of conformations.

In order to characterize the source of conformational flexibility, an independent but complementary classification in 2D of the whole data set was performed using multivariate statistical analysis (MSA) and multireference alignment (MRA) using IMAGIC (26). MSA followed by MRA was used to classify particles pre-aligned along their longitudinal axis. Further alignment and classification was carried out taking into account only individual lobes. Using the results of the previous classification, subsets of particles were selected in which the Pol lobe and Prim lobe could be identified. A mask was then used to classify and re-align the data taking into account only a specific lobe. Those averages in which a lobe displayed a unique and visually recognizable view were then further classified without the use of a mask or re-alignment.

Primer synthesis assays

Two types of primer initiation assays were performed: a primer capping assay that measured the ability of the polymerase domain of Pol α to cap an RNA primer with ddNTP, either as part of the primosome or when added *in trans* to the Prim lobe (Figure 5); a primer initiation assay that measured the effect on RNA primer synthesis of PriL-CTD addition *in trans* to a truncated Prim lobe missing the Fe-S domain (Figure 6B).

All assays contained 250 nM poly(dT)-70mer ssDNA as template DNA, 300 μM [α-^{32}P]-ATP, 50 mM TrisHCl pH 8.0, 5 mM $MgCl_2$, 2 mM DTT in a reaction volume of 20 μl. In the primer capping assay of Figure 5, ddATP was added at 100 μM and protein concentrations were: 100 nM primosome, 100 nM Prim complex and 100–300 nM of Polα_{cat} (added in stoichiometric ratios of 1:1, 1:2 and 1:3 to the Prim complex). In the primer synthesis assay of Figure 6B, protein concentrations were: 300 nM Prim complex, 300 nM PrimΔL_{CTD} complex and 300 nM to 3 μM of PriL-CTD (added in stoichiometric rations of 1:1, 1:5 and 1:10 to the PrimΔL_{CTD} complex). Reactions were incubated at 37°C for 30 min, the reaction products were separated in denaturing conditions on polyacrylamide gel and analyzed by phosphorimager.

Pull-down analysis

Amino acids 316–512 of PriL (PriL-CTD) were expressed in *E. coli* strain Rosetta 2 (DE3) from the pGAT2 vector (27) as an N-terminal His- and GST-tagged protein and purified using glutathione sepharose and size exclusion chromatography. Pull-down was performed by incubating 500 µl of 15 µM αCTD–B subunit complex with 150 µl of Glutathione Sepharose 4B beads that had been bound with an excess of PriL-CTD, in binding buffer 25 mM HEPES pH 7.0, 150 mM KCl, 1% BSA, 0.1% Igepal CA-630 and 2 mM TCEP at 4°C for 2 h. Beads were washed three times with binding buffer, once with 25 mM HEPES pH 7.0, 150 mM KCl and 2 mM TCEP and then resuspended in 200 µl LDS sample loading buffer (Invitrogen). Samples were run on SDS–PAGE gels, and visualised by coomassie staining and western blot, using an α-His_6 mAb (Abcam).

RESULTS

The primosome is a flexible dumbbell-shaped particle

We have biochemically reconstituted and purified the primosome of the yeast *S. cerevisiae* from recombinant versions of Pol α –B subunit complex produced in insect cells and bacterially expressed heterodimeric primase (see 'Materials and Methods' section for details). The N-terminal sequences of Pol α (1–348) and B subunit (1–245) were excluded from our analysis as they are generally poorly conserved and predicted to be predominantly disordered (Figure 1A). All structural analyses were

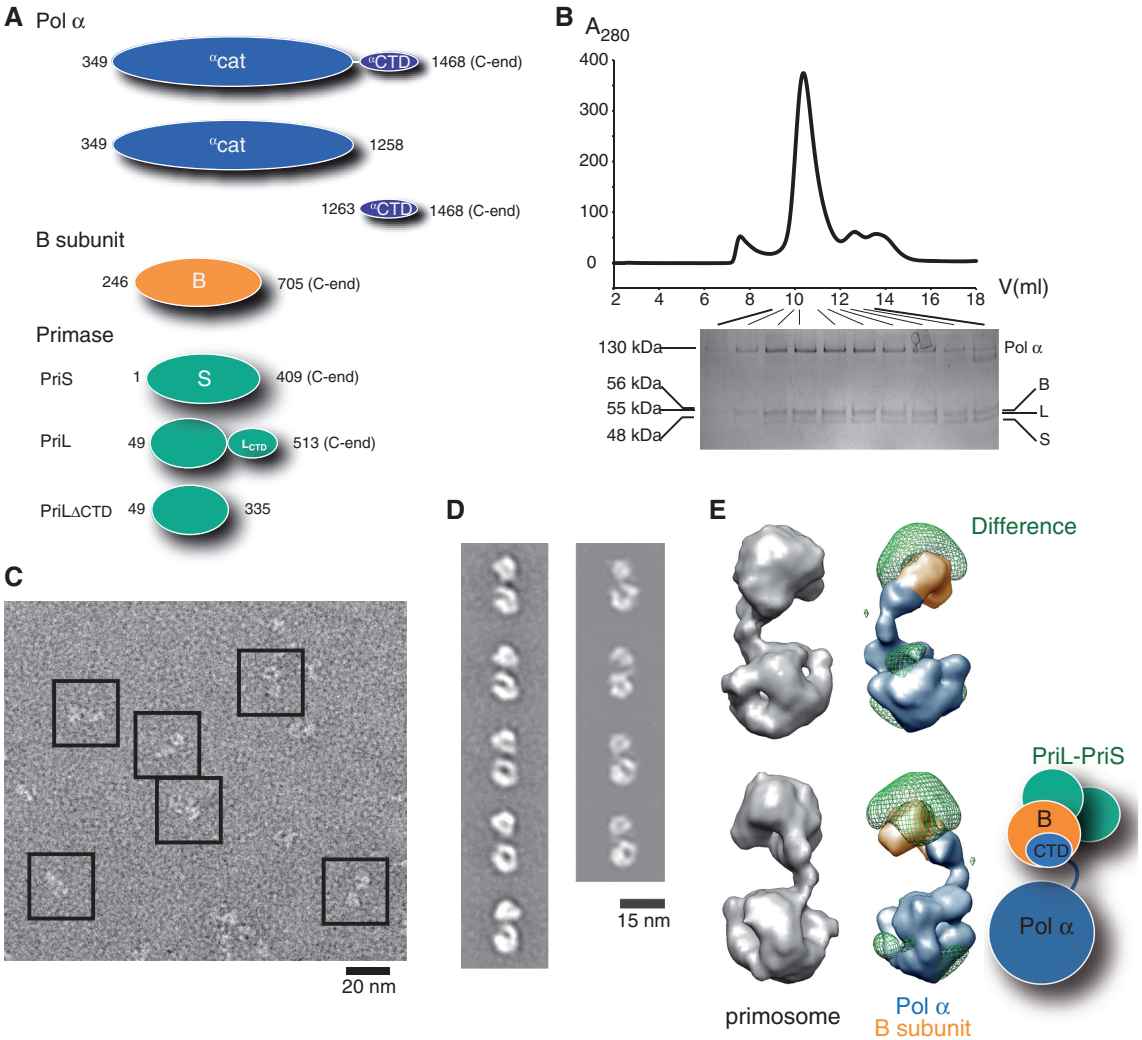

Figure 1. Biochemical reconstitution and electron microscopy analysis of the yeast primosome. (**A**) Cartoons of the different constructs used in this work. (**B**) Gel filtration chromatography of the reconstituted primosome prior to preparation of EM grids and SDS–PAGE analysis of peak fractions. The molecular weight of each subunit is indicated. (**C**) Representative electron micrographs obtained from a gel-filtered primosome sample. Selected raw particles are highlighted within squares. Scale bar represents 20 nm. (**D**) Reference-free 2D averages obtained from the EM images of the primosome (left panel) compared to projections of the Pol α–B subunit complex map (12) (right panel). Scale bar represents 15 nm. (**E**) 3D reconstruction of one conformation of the primosome, obtained after classification of a moderately homogenous subset of particles. A difference map between the primosome and the Pol α–B subunit complex (12) is represented as a green mesh superimposed to the structure of the Pol α–B subunit complex (see text for details of experimental procedure). This difference mapping defines the overall subunit organization in the primosome (right bottom panel).

performed on freshly gel-filtered primosome samples (Figure 1B). 17 628 single images of primosome particles were collected and a reference-free classification was performed, in order to increase the signal to noise ratio by averaging images corresponding to similar views of the complex (Figure 1C and D) (see Supplementary Figure S1 and Supplementary Table S1, for details on the image processing). The averages revealed an elongated, asymmetric particle similar in overall shape to the bilobal architecture previously determined for the Pol α–B subunit complex (12) (Figure 1D). These averages thus represent distinct side-view projections of the primosome rotating along its longitudinal axis. The conformation of the primosome particle observed by EM is in agreement with earlier hydrodynamic measurements that suggested a highly extended structure for the Pol α/primase complex (28).

Initial attempts to obtain a 3D structure of the primosome using the images obtained in the microscope failed since we consistently obtained reconstructions that lacked any connectivity between the two globular regions. We reasoned that the conformational flexibility already detected in the Pol α–B subunit complex could have increased in the primosome and thus we set up a multireference 3D classification strategy using methodology described before (25). The goal was to isolate and resolve the structure for a subset of particles corresponding to a certain 3D conformation of the primosome. Following this methodology (see 'Materials and Methods' section), we identified a subset of 3129 particles that could reconstruct a primosome at 25 Å resolution revealing substantial structural features and clear connectivity (Figure 1E). This subset of images was split and processed independently from scratch to remove the initial bias of the classification, confirming that the particles could be aligned in 3D with sufficient precision to conserve the structural details of the linker between the two lobes of the primosome. It is possible that the structure resulting from this multireference reconstruction strategy is a 3D average of closely related conformations rather than an entirely homogeneous conformation.

The primase interacts predominantly with the αCTD and the B subunit in the primosome

The structure of the primosome revealed a two-lobe architecture that was interpreted by comparison with the structure of the Pol α–B subunit complex (12). The larger lobe corresponded to the catalytic domain of the Pol α subunit, identified after comparison with the Pol α–B subunit complex and it was the only region matching the crystal structures of other DNA pol domains (12) (Figure 1E). In addition, this domain at the bottom end of the primosome was cropped from every single EM image and processed independently, which revealed 2D averages matching those of the Pol α subunit in the Pol α–B subunit complex (Supplementary Figure S3).

The structures of the primosome and the Pol α–B subunit complex were computationally aligned and each lobe was readjusted locally to account for the different orientation of the two lobes in each complex. After alignment, a difference map between both structures was calculated that revealed additional densities in the primosome complex corresponding to the primase subunits (Figure 1E, difference shown as a green mesh). This difference density accounted for roughly 30–35% of the total number of voxels in the reconstruction of the primosome, which correlates well with the percentage of mass corresponding to the primases within the complex. The primase was found prevalently associated with the αCTD and the B subunit, in a globular region that is separate from the polymerase domain of Pol α. This observation provides a rationale for biochemical reports concerning the mode of interaction of the primase within the Pol α/primase complex (29,30). It further provides an initial structural template on which to base mechanistic models for the synthesis of the RNA–DNA primers. Less prominent densities in the difference map were found in the vicinity of the catalytic domain of Pol α suggesting that some regions in the primases could extend to contact this subunit and/or that the conformation of Pol α is slightly different in the primosome and the Pol α–B subunit complex.

Highly flexible association between the polymerase and primase regions of the primosome

Using the multireference refinement strategy described before (Figure 1), we obtained the 3D structure of one conformation of the primosome observed in a subset of particles. We designed a complementary image classification strategy in 2D to characterize systematically the conformational complexity of the primosome using MSA and MRA of the images. In brief, the images of the data set were first aligned so that the globular region containing the polymerase domain of Pol α (hereinafter referred to as 'Pol lobe') was placed at the bottom end and the αCTD–B subunit-primase (hereinafter 'Prim lobe') at the top end. A computational mask was then applied to each single image to restrict the information used during image classification to the Pol lobe. Several classes containing single images with an identical view of the Pol lobe were obtained (Figure 2A, each row representing one of these classes). For each of these subgroups, an additional round of classification was then performed removing the mask so that the full image of the primosome was used for classification, revealing multiple orientations of the Prim lobe for each static view of the Pol lobe. The analysis showed that the Prim lobe occupied a large range of different positions relative to a single orientation of the catalytic Pol lobe. Thus, the primosome possesses a high degree of plasticity in the inter-lobe connection, potentially giving rise to a large number of relative orientations of the two lobes (Figure 2A, right panel). The conformational flexibility of the primosome particle is conveniently visualized treating each average as a frame of a movie (Supplementary Movie S1–6).

Despite the extensive image classification performed, the structural features of the Prim lobe in these averages remained blurred compared to a well defined pol lobe, suggesting that several rotational states of the Prim lobe were still present in each subgroup of particles. This was confirmed by additional classification of particles with an

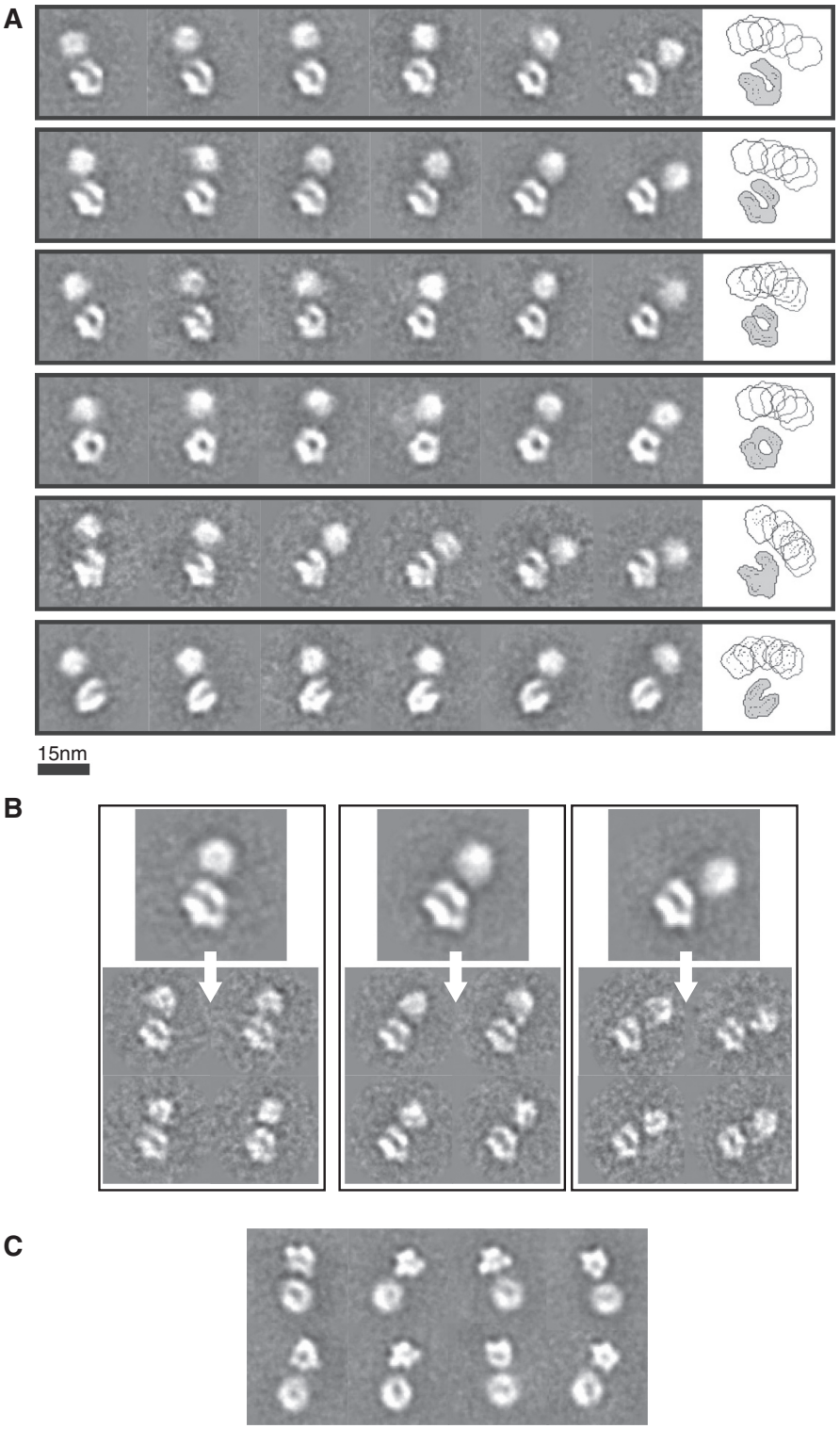

Figure 2. Conformational flexibility of the eukaryotic primosome. (**A**) Collection of 2D reference-free averages of the primosome. Each row shows a set of averages where the Pol lobe is oriented according to the same view. The conformational flexibility of the primosome is highlighted by a cartoon outline showing the superposition of all averages in a row. Scale bar represents 15 nm. (**B**) Three selected class averages in panel A were further classified to demonstrate the degree of rotational heterogeneity still present in the average: the position of the Prim lobe is determined by a combination of tilt and rotation relative to the Pol lobe. (**C**) Reference-free classification of the data set after masking out the information of the Pol lobe. Alignment of the Prim lobe results in blurring of the Pol lobe, an additional indication of the high degree of interlobe flexibility of the primosome. (See also Supplementary Movie S1–S6).

apparently fixed orientation between the lobes, which revealed further heterogeneity due to rocking of the Prim lobe. (Figure 2B). We repeated the image classification strategy, masking the Pol lobe and focusing on the Prim lobe. This time, for each well-defined orientation of the Prim lobe (Figure 2C, top lobe), a blurred image of the Pol lobe was obtained (Figure 2C, bottom lobe), which further confirmed that the conformational freedom of the primosome particle derives from a combination of rocking and twisting motion of the two lobes relative to each other.

Geometrical analysis of the primosome

The realization that the two catalytic centers of the primosome reside in physically distant regions of the particle has important implications for our functional understanding of the mechanism of synthesis of the RNA and DNA portions of the primer. We exploited the extensive image classification of Figure 2A to perform a simple geometric analysis, which allowed us to extract some basic physical properties of the primosome particle (Figure 3A). By approximating the Pol and Prim lobes as circular regions and measuring the distance between the centers of the circles in each particle, we estimated an average interlobe distance of 112 Å (Figure 3B).

Despite the high degree of relative mobility between lobes, the particle averages of Figure 2A show that the range of positions occupied by the Prim lobe spans an angle no larger than ~70° relative to the Pol lobe. Based on simple geometric considerations, it is possible to estimate the size of the linker that tethers the lobes from the

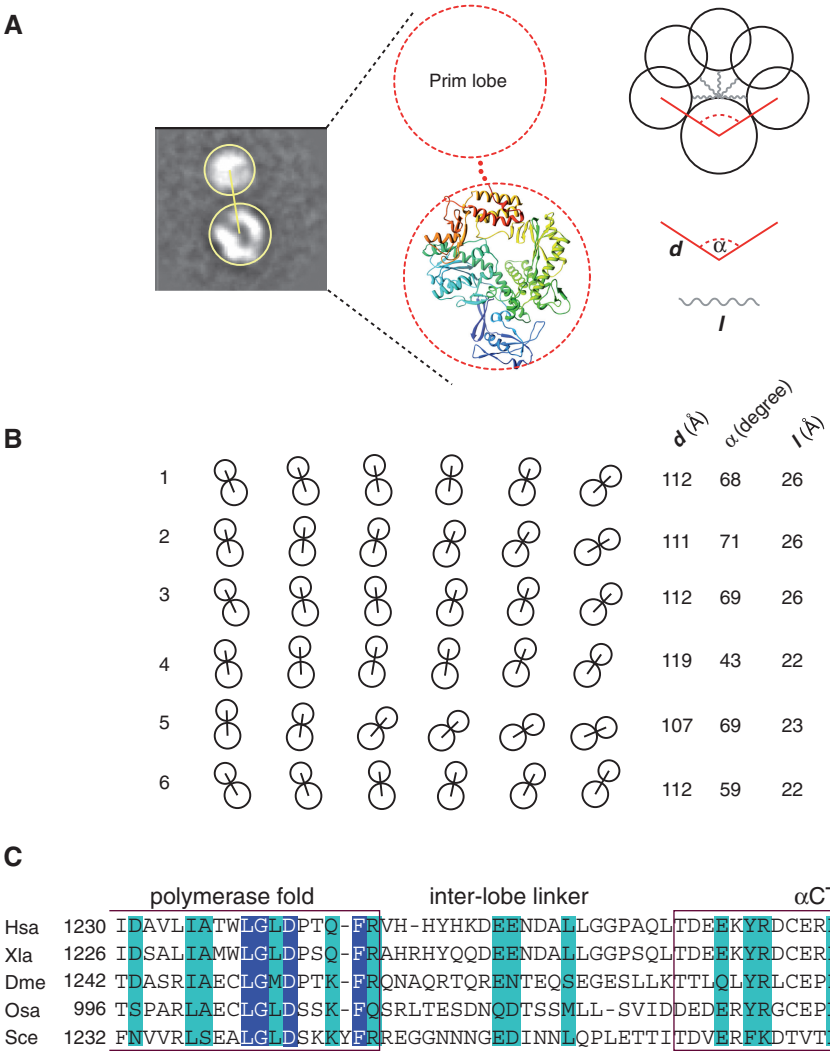

Figure 3. Geometric analysis of the yeast primosome. (**A**) 2D averages of the primosome can be approximated as two circular lobes connected by a flexible linker. Depicted in the Pol lobe is the structure of a related archaeal polymerase (unpublished PDB entry: 3A2F). The flexibility can be characterized by the geometrical parameters *d* for interlobe distance, **α** for the interlobe angle in a set of related averages and *l* for linker size. (**B**) Geometrical outlines of the 36 2D averages of the yeast primosome in Figure 2A. For each set, the average interlobe distance *d*, the interlobe angle **α** and the estimated size of the interlobe linker *l* are reported. (**C**) Multiple sequence alignment of the amino acid sequence linking the polymerase domain of Pol α to its carboxy-terminal domain (αCTD) (Hsa: *Homo sapiens*; Xla: Xenopus laevis; Dme: *Drosophila melanogaster*; Osa: *Oryza sativa*; Sce: *Saccharomyces cerevisiae*). The boundaries for the polymerase domain and the αCTD were determined based on the crystal structures of yeast Pol δ (37) and yeast αCTD (12), respectively. Identical amino acids are highlighted in blue and conserved amino acids in green.

observed angular range of relative interlobe positions. Such an analysis yields an average linker length of 24 Å, a relatively modest distance that could be spanned by as little as nine amino acids in fully extended, beta conformation. This estimate is in good agreement with the known size of the linker sequence connecting polymerase and carboxy-terminal domains of Pol α (see Figure 3C).

The eukaryotic primase is an elongated subunit that promotes inter-lobe flexibility of the primosome

In order to improve the structural definition of the Prim lobe, we reconstituted biochemically and analyzed by EM a complex comprising αCTD, the B subunit and the primase (hereinafter referred to as 'Prim complex'). Reference-free 2D averages of 11 088 particles of the Prim complex revealed an elongated structure, formed by a larger globular region with a smaller oblong protrusion (Figure 4A). The features of the globular portion of the Prim complex were similar to those of the Prim lobe in the primosome (comprising αCTD, B subunit and the primase subunits). This similarity was supported by the high correlation (>0.9) of the comparison between averages of the Prim lobe and the globular region of the Prim complex (Supplementary Figure S3). Strikingly, the longitudinal dimension for the Prim complex was

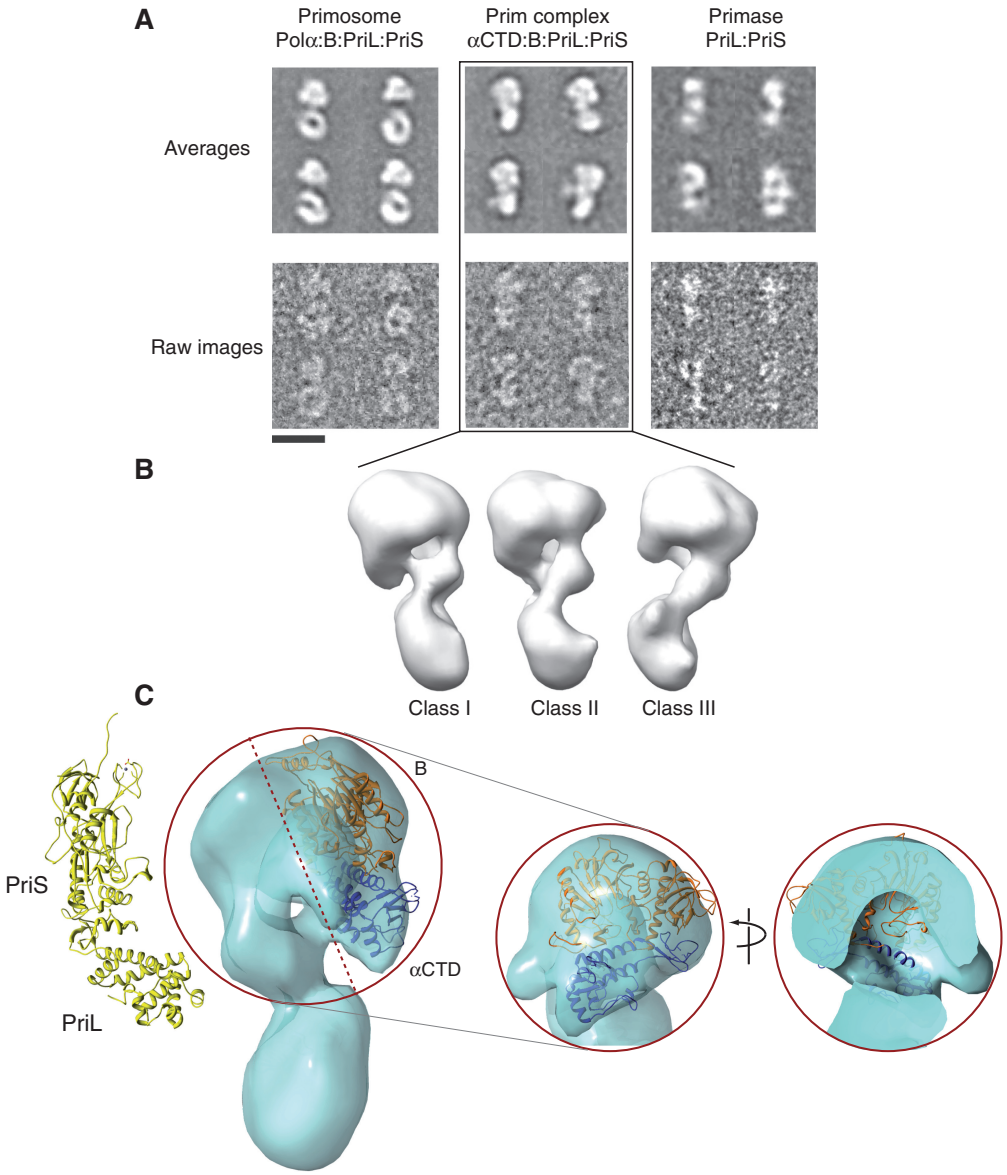

Figure 4. 3D structure of yeast Prim complex. (**A**) Selected reference-free 2D averages and the corresponding raw images of the different complexes after observation in the electron microscope, shown at identical magnification. Bar represents 15 nm. (**B**) 3D-structures of the Prim complex obtained by maximum-likelihood methods (see text for details). (**C**) Fitting of the αCTD–B subunit complex in the density of the Prim complex. The αCTD and B subunits are shown as blue and orange ribbon, respectively. The density of the Prim complex is in cyan. The crystal structure of a truncated form of the heterodimeric archaeal primase from *Sulfolobus solfataricus* (PDB: 1ZT2) is shown as yellow ribbon next to the Prim complex density. ('B'–B subunit).

significantly larger than the Prim lobe in the primosome (Figure 4A). Indeed, a subtraction map between averages of the Prim lobe and the Prim complex after alignment revealed that, whereas the larger globular region was similar in both complexes, difference density was placed at the oblong protrusion (Supplementary Figure S3).

3D reconstruction of the Prim complex confirmed that it comprises a larger, globular domain and a smaller, elongated region (see 'Materials and Methods' section for details) (Figure 4B). 3D classification of the images in three related but different conformations by maximum-likelihood methods revealed variability in the position of the smaller region relative to the large globular region of the Prim complex. A channel that expands in a larger, internal cavity crosses the globular region and divides it in two halves of roughly equal size. A crystallographic model of the αCTD–B subunit complex (12) was fit with the structure of the Prim complex using computational tools (23,24). All top solutions convincingly fit the αCTD–B subunit complex in one side of the globular domain (cross-correlation >0.6) and these were also the only solutions placing the atomic structure entirely within the EM map (Figure 4C). No structural information is currently available for the eukaryotic primase, with the exception of the carboxy-terminal domain of the large subunit (14,15). The region in the Prim complex that remains unoccupied after fitting the αCTD–B subunit complex could then be assigned to the primase subunits. The eukaryotic primase displays an elongated structure within the Prim complex (Figure 4C). Indeed, EM images of isolated yeast primase revealed a very extended shape, but thinner than that of the Prim complex; the difference in size can be accounted for by the B-subunit and the αCTD (Figure 4A). In addition, a crystallographic model comprising a portion of an archaeal heterodimeric primase displays also an extended conformation (Figure 4C) (5), which agrees with the shape of the region of the Prim complex that remains available after fitting of the αCTD–B subunit complex (12). Nevertheless, we did not have sufficient information to unambiguously fit the structure of the archaeal primase within the Prim complex.

Available evidence identifies PriL as the subunit that anchors the primase to Pol α and shows that the interaction with the primase is mediated by the αCTD (29,31,32). These experimental constraints can be satisfied by assigning PriS to the upper half of the globular region of the Prim complex and PriL to the lower half, directly facing the αCTD. Intriguingly, the presence of residual density protruding from the larger globular region of the Prim complex suggests that the area of Pol α contacted by the primase might extend beyond the αCTD and include the linker region between polymerase domain and αCTD and/or other regions of Pol α. A specific interaction between the primase and the Pol α linker sequence might be responsible for the greatly increased interlobal mobility observed in the primosome relative to the Pol α–B subunit complex (12).

Flexible tethering of Prim and Pol lobes contributes to the efficient transfer of RNA primers

The observed organization of the primosome as two physically independent catalytic centers connected by a highly flexible linker provides a structural basis for understanding the mechanism of primer transfer. We set out to compare the efficiency of primer transfer in the intact primosome and in a sample containing the Prim complex and the polymerase domain of Pol α (Polα_{cat}). In the latter sample, the lobes of the primosome are physically separated and primer transfer must necessarily take place *in trans*. The experiment exploited the known tendency of the eukaryotic primase to generate RNA multimers *in vitro* by repeated extension of unit-length primers. We designed a primer capping assay that measured the efficiency of addition of di-deoxyadenosine triphosphate (ddATP) to the unit-length RNA primer by Pol α: the extent of residual RNA multimer formation in reactions that contained ddATP would correlate inversely with the efficiency of primer transfer between primase and Pol α. The experiment showed that a mix of Prim complex and Pol α_{cat} was clearly less efficient in primer capping than the primosome, even when Pol α_{cat} was added in stoichiometric excess (Figure 5).

The carboxy-terminal portion of PriL (PriL-CTD) has a critical role in RNA primer synthesis (7,8). A tentative assignment of the PriL-CTD position in the Prim lobe was made by comparing EM images of the Prim complex and the PrimΔL_{CTD}, lacking the PriL-CTD. The PriL-CTD was identified as a clear spot occupying a range of related positions relative to the longitudinal axis of the Prim complex, indicative of a mobile tethering to the rest of the primase molecule (Figure 6A). PriL-CTD was not detected in the 3D structure of the primosome (Figure 1E) most likely because the images used in the reconstruction remained sufficiently heterogeneous to average out its density.

The PrimΔL_{CTD} complex displayed a greatly diminished level of RNA primer synthesis relative to the Prim complex, in agreement with previous observations that the PriL-CTD has a critical role in primer initiation (Figure 6B) (7). Interestingly, reconstitution of the Prim complex *in trans* by addition of PriL-CTD to PrimΔL_{CTD} caused a noticeable increase in the ability of the PrimΔL_{CTD} to extend the unit-size primer, suggestive of a functional involvement of the PriL-CTD beyond the initiation stage. We sought to determine whether this functional effect could be dependent on a direct association of the PriL-CTD with the PrimΔL_{CTD} during primer synthesis. The PriL-CTD has only a weak affinity for nucleic acid, so it is unlikely to interact independently with the nascent template-bound RNA primer at the concentrations used in the assay (14). Alternatively, the effect might be mediated by a protein–protein contact with the PrimΔL_{CTD}. Indeed, we detected an interaction by pull-down assay between the PriL-CTD and the αCTD–B complex (Figure 6C). Although this interaction is probably too weak to represent the principal mode of interaction between the primase and the Pol α–B complex, it might

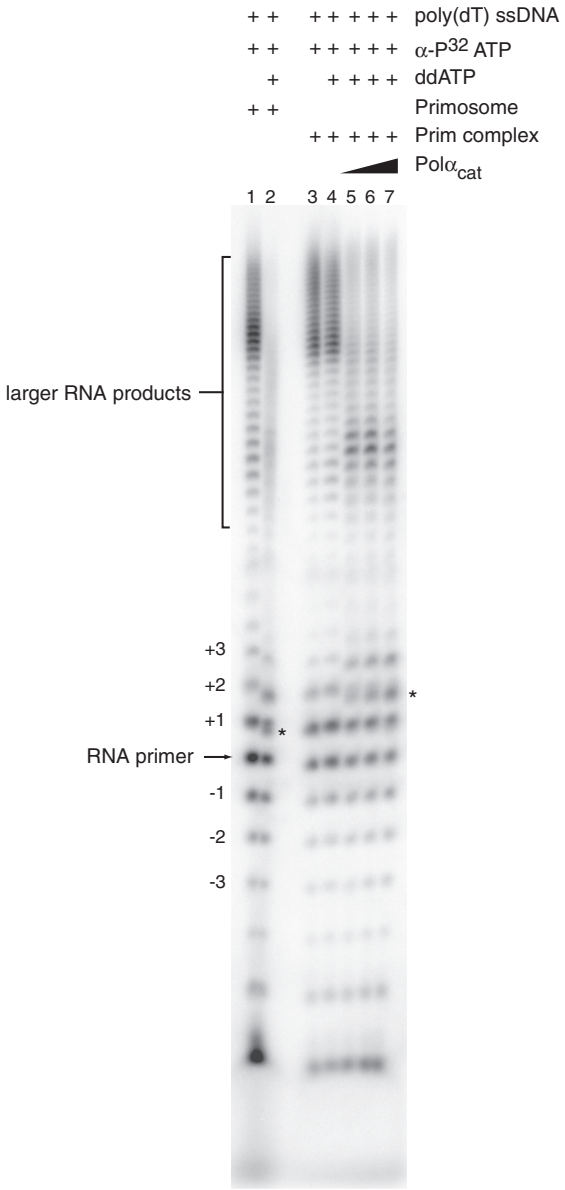

Figure 5. Functional analysis of yeast primosome. The primer capping assay measures the efficiency of ddATP addition to the RNA primer by Pol α's catalytic domain (Pol α_{cat}), as part of the primosome or when added *in trans* to the Prim complex. Lane 1: primosome activity in the presence of ATP (control); lane 2: primosome activity in the presence of ATP and ddATP; lane 3; Prim complex activity in the presence of ATP (control); lane 4: Prim complex activity in the presence of ATP and ddATP (control); lanes 5–7: Prim complex activity in the presence of ATP, ddATP and increasing amounts of Pol α_{cat}, in stoichiometric ratios of 1:1, 1:2 and 1:3. The asterisks mark the first appearance of an RNA primer capped with ddATP for the primosome and the Prim complex.

play a role in orienting the PriL-CTD during primer synthesis.

DISCUSSION

The semi-discontinuous nature of DNA replication means that nucleic acid synthesis must be continuously primed on the lagging strand. In eukaryotes, the functions of RNA primer synthesis and initial elongation are coupled within the primase/Pol α complex or primosome. The physical association of primase and polymerase activities provides the basis for their tight functional coupling. Indeed, a large body of experimental evidence points to an intramolecular mechanism of RNA primer transfer between active sites of primase and Pol α in the primosome (31,33–35). Thus, after unit-length primer synthesis by the primase, the 3′-terminus of the template-bound primer undergoes an internal translocation to the active site of Pol α, without dissociating in solution.

Despite the biochemical evidence of intramolecular hand-off, the nature of the switch that transfers the primer between primase and Pol α is currently unknown. Here, we have provided the first experimental evidence for the 3D architecture of the eukaryotic primosome. We show that the primosome is organized as a dumbbell-shaped particle with flexibly connected lobes. The catalytic domain of Pol α resides in one lobe, whereas the other lobe is formed by the interaction of the αCTD, the B subunit and the primase. Although the bulk of the primase is clearly associated in a globular region with αCTD and B subunit, EM analysis of the isolated Prim lobe and the primase show an elongated shape, in agreement with previous crystallographic evidence of the related archaeal primase (5). A remarkable feature of the eukaryotic primosome is the highly flexible nature of the physical connection between Prim and Pol lobes, which contrasts with the more limited flexibility observed previously in the Pol α–B complex (12). It is possible that specific, local interactions between the primase and the Pol α at or near its linker region could be responsible for the increased interlobe flexibility. In support of this model, PriL binds Pol α after simultaneous co-expression of primosome subunits in COS-1 cells (29,30).

Our structural and functional data show that the molecular architecture of the primosome as two physically independent, flexibly connected catalytic modules represents the physical basis for primer transfer from the primase to Pol α (Figure 7). Although primer transfer can take place in mixtures of purified Prim and Pol complexes that are not covalently linked, the efficiency of primer transfer is greatly increased within the primosome (Figure 5). These findings are compatible with alternative functional models of how primase and Pol α cooperate in the assembly of the RNA–DNA primers. One possibility is that the physical link between lobes would increase RNA transfer efficiency, by minimizing the rate at which the RNA primer diffuses between the active sites of primase and Pol α. In this case, the observed linker flexibility would allow the two catalytic modules to operate independently, similar to the mechanism proposed for the primase–helicase of bacteriophage T7 (36).

Alternatively, the flexible connection between lobes in the primosome could be a functional feature of a concerted mechanism of primer hand-off between primase and Pol α. Synthesis of a unit-length primer by the primase would trigger a specific rearrangement of the

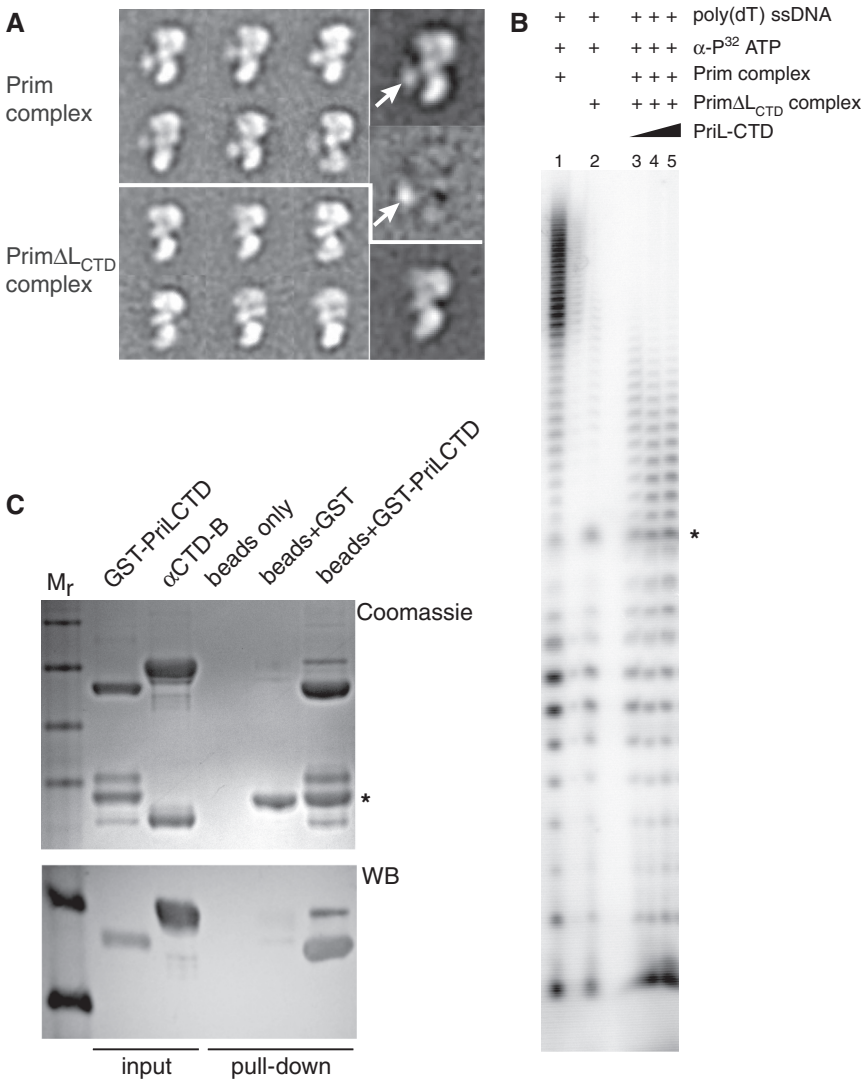

Figure 6. Structural and functional analysis of the PriL-CTD. (**A**) 2D reference-free averages of the Prim complex and the PrimΔL$_{CTD}$ complex. The putative position of the PriL-CTD in the Prim complex is indicated by an arrow. (**B**) Functional analysis of the Prim complex. The ability of the Prim complex to synthesise an RNA primer was compared to that of the PrimΔL$_{CTD}$ when the PriL-CTD was added *in trans* to the reaction, in stoichiometric ratios of 1:1, 1:5 and 1:10. The band position marked by the asterisk is a gel artifact caused by the gel running dye. (**C**) GST pull-down analysis of the interaction between PriL-CTD and the αCTD–B subunit complex. The top panel shows the Coomassie staining of the gel and the bottom panel the western blot with anti-His antibodies. The asterisk marks the position of the GST protein.

primosome lobes, causing the engagement of Pol α's active site with the 3′-terminus of the RNA primer. Indeed, it has been proposed that primer completion is the signal for the switch from primase to polymerase activity (34,35). A separation of over 100 Å between the centers of the primosome lobes implies that a large-scale conformational rearrangement would necessarily be an integral part of a concerted hand-off mechanism (Figure 7).

At this stage, there is insufficient evidence to reach a firm conclusion concerning the nature of the mechanism of primer transfer within the primosome. The multiple priming events required to sustain replication of the lagging strand imply that the primosome must cycle continuously and rapidly through the steps of primer synthesis, transfer, elongation and release. Such functional behaviour would naturally call for a high degree of coordination between the catalytic activities of the primosome, pointing to the existence of an integrated process of primer hand-over between primase and Pol α.

In conclusion, the evidence presented here provides the first structural model of the eukaryotic primosome and an initial insight into the mechanism of RNA–DNA primer assembly during initiation of nucleic acid synthesis in eukaryotic replication. Future efforts will be aimed at characterizing in atomic detail each stage of the primosome's catalytic cycle.

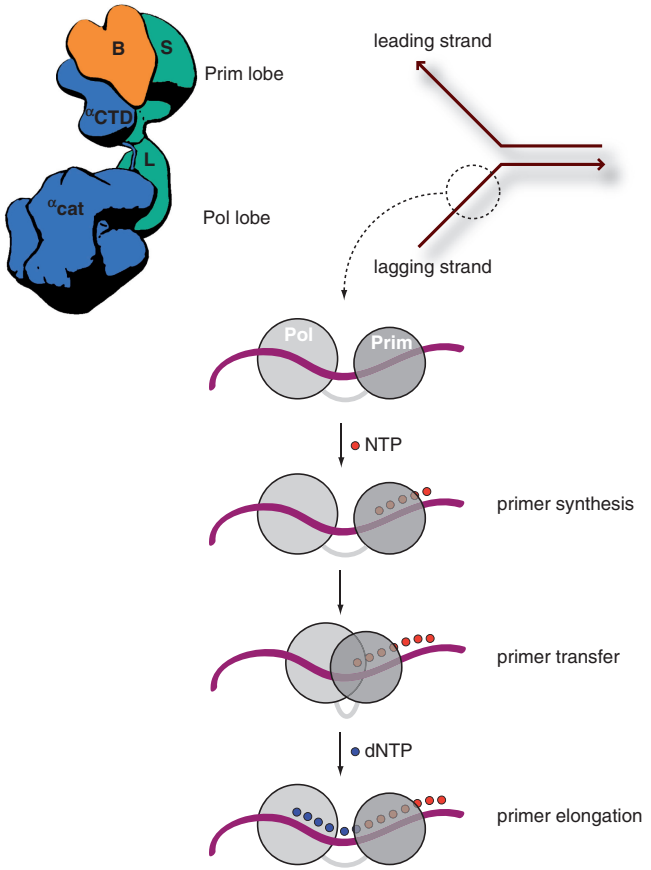

Figure 7. Model for the molecular architecture of the primosome. The model is based on the observations that the primase and polymerase activities reside in separate regions of the primosome, connected by a highly flexible linker ('B'–B subunit; 'S'–PriS; 'L'–PriL; $^{\alpha}$CTD and $^{\alpha}$cat–C-terminal and catalytic domain of Pol α). The elongated shape of the primase can contact in principle the Pol lobe. Since the large subunit of the primase binds Pol α, PriL has been tentatively placed closer to Pol α (29,30). A schematic diagram of the steps of RNA–DNA primer synthesis, based on a hypothetical rearrangement of Pol and Prim lobes during primer transfer is also shown.

SUPPLEMENTARY DATA

Supplementary Data are available at NAR Online.

FUNDING

Spanish Ministry of Science and Innovation (SAF2008-00451 to O.L.); the 'Red Temática de Investigación Cooperativa en Cáncer (RTICC)' from the 'Instituto de Salud Carlos III' (RD06/0020/1001 to O.L.); the Human Frontiers Science Program (RGP39/2008 to O.L. and E.N.); a Wellcome Trust Senior Fellowship award in Basic Biomedical Sciences (to L.P.); a FPI fellowship from the Spanish Ministry of Science and Innovation to MAR-C; a JAE-DOC contract of the 'Consejo Superior de Investigaciones Científicas (CSIC)' and a 'Juan de la Cierva' contract from the Spanish Ministry of Science to BGA; EN is a Howard Hughes Medical Institute Investigator. Funding for open access charge: Spanish Ministry of Science and Innovation (SAF2008-00451 to O.L.).

Conflict of interest statement. None declared.

REFERENCES

1. Frick,D.N. and Richardson,C.C. (2001) DNA primases. *Annu. Rev. Biochem.*, **70**, 39–80.
2. Kuchta,R.D. and Stengel,G. (2010) Mechanism and evolution of DNA primases. *Biochim. Biophys. Acta*, **1804**, 1180–1189.
3. Hamdan,S.M. and van Oijen,A.M. (2010) Timing, coordination, and rhythm: acrobatics at the DNA replication fork. *J. Biol. Chem.*, **285**, 18979–18983.
4. Burgers,P.M. (2009) Polymerase dynamics at the eukaryotic DNA replication fork. *J. Biol. Chem.*, **284**, 4041–4045.
5. Lao-Sirieix,S.H., Nookala,R.K., Roversi,P., Bell,S.D. and Pellegrini,L. (2005) Structure of the heterodimeric core primase. *Nat. Struct. Mol. Biol.*, **12**, 1137–1144.
6. Lao-Sirieix,S.H., Pellegrini,L. and Bell,S.D. (2005) The promiscuous primase. *Trends Genet.*, **21**, 568–572.
7. Klinge,S., Hirst,J., Maman,J.D., Krude,T. and Pellegrini,L. (2007) An iron-sulfur domain of the eukaryotic primase is essential for RNA primer synthesis. *Nat. Struct. Mol. Biol.*, **14**, 875–877.
8. Weiner,B.E., Huang,H., Dattilo,B.M., Nilges,M.J., Fanning,E. and Chazin,W.J. (2007) An iron-sulfur cluster in the C-terminal domain of the p58 subunit of human DNA primase. *J. Biol. Chem.*, **282**, 33444–33451.
9. Muzi-Falconi,M., Giannattasio,M., Foiani,M. and Plevani,P. (2003) The DNA polymerase alpha-primase complex: multiple functions and interactions. *ScientificWorldJournal*, **3**, 21–33.
10. Stillman,B. (2008) DNA polymerases at the replication fork in eukaryotes. *Mol. Cell*, **30**, 259–260.
11. Johansson,E. and Macneill,S.A. (2010) The eukaryotic replicative DNA polymerases take shape. *Trends Biochem. Sci.*, **35**, 339–347.
12. Klinge,S., Nunez-Ramirez,R., Llorca,O. and Pellegrini,L. (2009) 3D architecture of DNA Pol alpha reveals the functional core of multi-subunit replicative polymerases. *EMBO J.*, **28**, 1978–1987.
13. Augustin,M.A., Huber,R. and Kaiser,J.T. (2001) Crystal structure of a DNA-dependent RNA polymerase (DNA primase). *Nat. Struct. Biol.*, **8**, 57–61.
14. Sauguet,L., Klinge,S., Perera,R.L., Maman,J.D. and Pellegrini,L. (2010) Shared active site architecture between the large subunit of eukaryotic primase and DNA photolyase. *PLoS ONE*, **5**, e10083.
15. Vaithiyalingam,S., Warren,E.M., Eichman,B.F. and Chazin,W.J. (2010) Insights into eukaryotic DNA priming from the structure and functional interactions of the 4Fe-4S cluster domain of human DNA primase. *Proc. Natl Acad. Sci. USA*, **107**, 13684–13689.
16. Mindell,J.A. and Grigorieff,N. (2003) Accurate determination of local defocus and specimen tilt in electron microscopy. *J. Struct. Biol.*, **142**, 334–347.
17. Heymann,J.B. and Belnap,D.M. (2007) Bsoft: image processing and molecular modeling for electron microscopy. *J. Struct. Biol.*, **157**, 3–18.
18. Ludtke,S.J., Baldwin,P.R. and Chiu,W. (1999) EMAN: semiautomated software for high-resolution single-particle reconstructions. *J. Struct. Biol.*, **128**, 82–97.
19. Ranson,N.A., Farr,G.W., Roseman,A.M., Gowen,B., Fenton,W.A., Horwich,A.L. and Saibil,H.R. (2001) ATP-bound states of GroEL captured by cryo-electron microscopy. *Cell*, **107**, 869–879.
20. Scheres,S.H., Nunez-Ramirez,R., Sorzano,C.O., Carazo,J.M. and Marabini,R. (2008) Image processing for electron microscopy single-particle analysis using XMIPP. *Nat. Protoc.*, **3**, 977–990.
21. Scheres,S.H., Valle,M., Nunez,R., Sorzano,C.O., Marabini,R., Herman,G.T. and Carazo,J.M. (2005) Maximum-likelihood multi-reference refinement for electron microscopy images. *J. Mol. Biol.*, **348**, 139–149.
22. Scheres,S.H., Gao,H., Valle,M., Herman,G.T., Eggermont,P.P., Frank,J. and Carazo,J.M. (2007) Disentangling conformational

states of macromolecules in 3D-EM through likelihood optimization. *Nat. Methods*, **4**, 27–29.
23. Garzon,J.I., Kovacs,J., Abagyan,R. and Chacon,P. (2007) ADP_EM: fast exhaustive multi-resolution docking for high-throughput coverage. *Bioinformatics*, **23**, 427–433.
24. Goddard,T.D., Huang,C.C. and Ferrin,T.E. (2007) Visualizing density maps with UCSF Chimera. *J. Struct. Biol.*, **157**, 281–287.
25. Chen,D.H., Song,J.L., Chuang,D.T., Chiu,W. and Ludtke,S.J. (2006) An expanded conformation of single-ring GroEL-GroES complex encapsulates an 86 kDa substrate. *Structure*, **14**, 1711–1722.
26. van Heel,M., Harauz,G., Orlova,E.V., Schmidt,R. and Schatz,M. (1996) A new generation of the IMAGIC image processing system. *J. Struct. Biol.*, **116**, 17–24.
27. Peranen,J., Rikkonen,M., Hyvonen,M. and Kaariainen,L. (1996) T7 vectors with modified T7lac promoter for expression of proteins in Escherichia coli. *Anal. Biochem.*, **236**, 371–373.
28. Goulian,M. and Heard,C.J. (1989) Intact DNA polymerase alpha/primase from mouse cells. Purification and structure. *J. Biol. Chem.*, **264**, 19407–19415.
29. Mizuno,T., Yamagishi,K., Miyazawa,H. and Hanaoka,F. (1999) Molecular architecture of the mouse DNA polymerase alpha-primase complex. *Mol. Cell. Biol.*, **19**, 7886–7896.
30. Smith,R.W. and Nasheuer,H.P. (2002) Control of complex formation of DNA polymerase alpha-primase and cell-free DNA replication by the C-terminal amino acids of the largest subunit p180. *FEBS Lett.*, **527**, 143–146.
31. Copeland,W.C. and Wang,T.S. (1993) Enzymatic characterization of the individual mammalian primase subunits reveals a biphasic mechanism for initiation of DNA replication. *J. Biol. Chem.*, **268**, 26179–26189.
32. Longhese,M.P., Jovine,L., Plevani,P. and Lucchini,G. (1993) Conditional mutations in the yeast DNA primase genes affect different aspects of DNA metabolism and interactions in the DNA polymerase alpha-primase complex. *Genetics*, **133**, 183–191.
33. Eki,T. and Hurwitz,J. (1991) Influence of poly(ADP-ribose) polymerase on the enzymatic synthesis of SV40 DNA. *J. Biol. Chem.*, **266**, 3087–3100.
34. Kuchta,R.D., Reid,B. and Chang,L.M. (1990) DNA primase. Processivity and the primase to polymerase alpha activity switch. *J. Biol. Chem.*, **265**, 16158–16165.
35. Sheaff,R.J., Kuchta,R.D. and Ilsley,D. (1994) Calf thymus DNA polymerase alpha-primase: "communication" and primer-template movement between the two active sites. *Biochemistry*, **33**, 2247–2254.
36. Toth,E.A., Li,Y., Sawaya,M.R., Cheng,Y. and Ellenberger,T. (2003) The crystal structure of the bifunctional primase-helicase of bacteriophage T7. *Mol. Cell.*, **12**, 1113–1123.
37. Swan,M.K., Johnson,R.E., Prakash,L., Prakash,S. and Aggarwal,A.K. (2009) Structural basis of high-fidelity DNA synthesis by yeast DNA polymerase delta. *Nat. Struct. Mol. Biol.*, **16**, 979–986.